Supplementary Information：

Long-term monitoring of intravital biological processes using fluorescent protein-assisted NIR-II imaging

Chen et al

Long-term monitoring of intravital biological processes using fluorescent protein-assisted NIR-II imaging

Supplementary Figure 1. iRFPs purification.

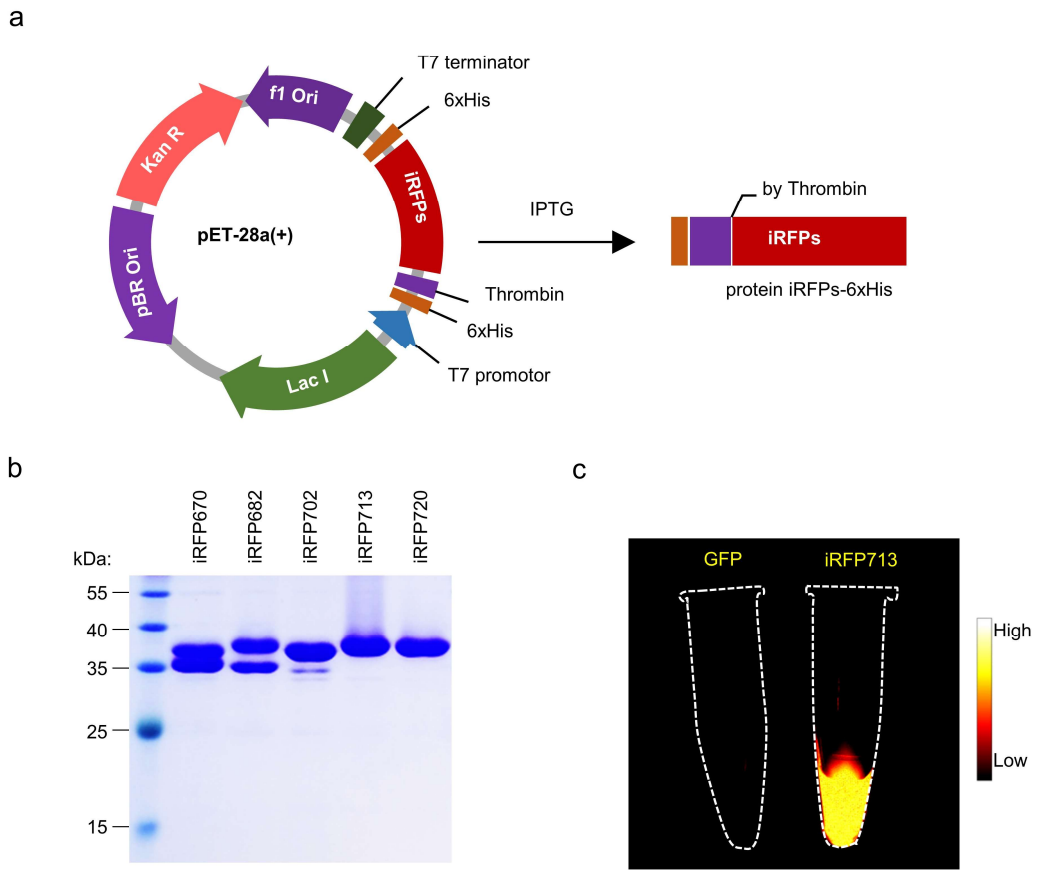

(**a**) Diagram of the recombinant pET28a-iRFPs-6xHis plasmid, for expression of N-terminally 6xHis-tagged proteins with a thrombin site. (**b**) Coomassie blue staining of purified recombinant iRFPs. Experiment was performed in biological triplicate. (**c**) A NIR-II fluorescence image of purified recombinant GFP protein and iRFP713 protein with 690 nm excitation and 900 nm LP filters. Exposure times: 10 ms. Source data are provided as a Source Data file.

Supplementary Figure 2. NIR-II fluorescence imaging of stable iRFP713-expressing cells.

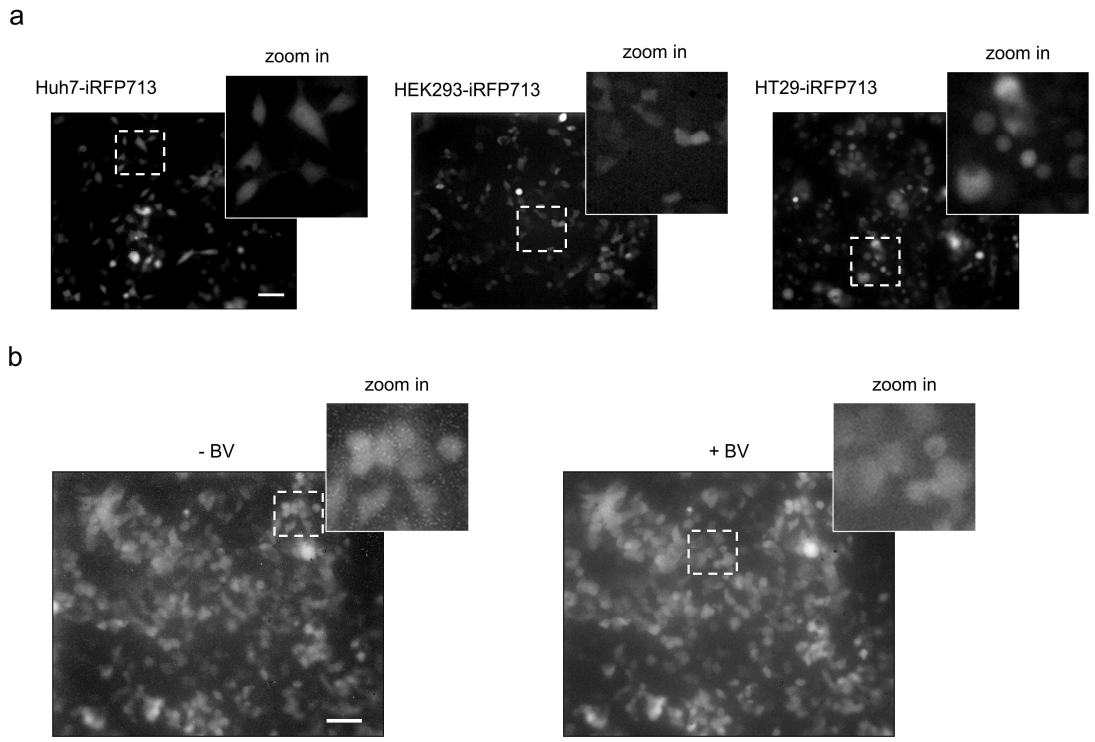

(**a**) NIR-II fluorescence wide-field microscopic images of various iRFP713 stably transfected cells, including Huh7-iRFP713, HEK293-iRFP713, and HT29-iRFP713. (**b**) NIR-II fluorescence images of HEK293-iRFP713 cells without and with addition of 25 μM BV for 2 hours. Each cell experiment was performed three times independently in duplicate each time. Cells were imaged under 690 nm excitation, using 900 nm LP filters. Scale bar: 50 μm.

Supplementary Figure 3. NIR-II fluorescence imaging of mice infected with iRFP713-encoding adenovirus.

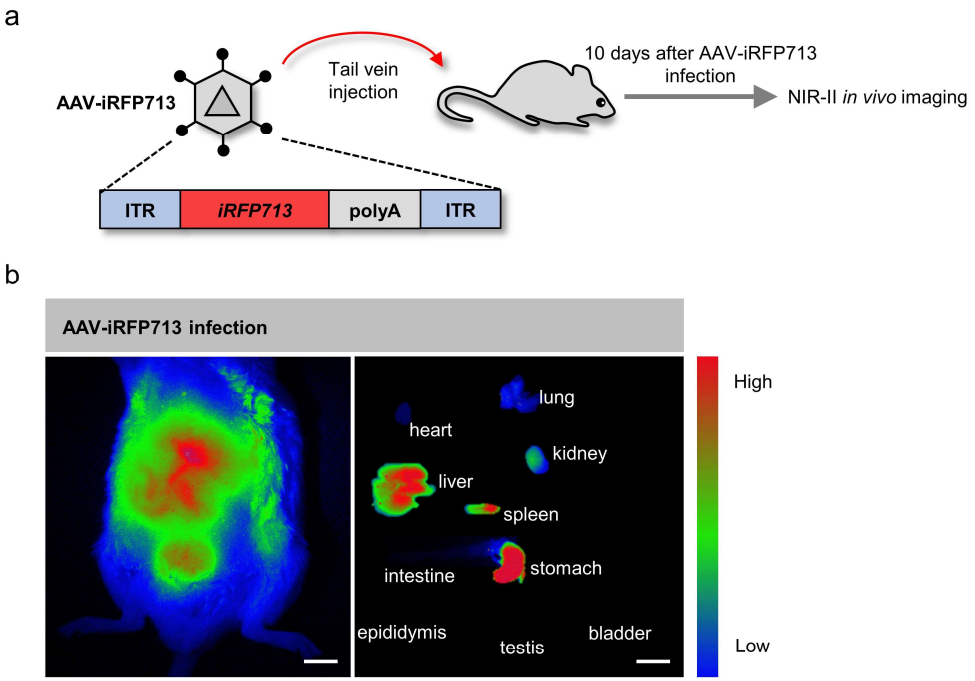

(**a**) Diagram representing the iRFP713-encoding adenovirus (AAV-iRFP713) and the experimental design used in the corresponding animal studies. C57BL/6 mice (male 6-8 weeks old) were intravenously injected with $2x10^9$ infectious units of the iRFP713-encoding adenovirus. (**b**) Ten days after injection, iRFP713-infected mice and their isolated organs were imaged using a 690 nm laser and 900 nm LP filter for excitation and emission, respectively. Exposure times: 50 ms. Scale bars: 2 mm (**b, left**) and 1 cm (**b, right**).

Supplementary Figure 4. Construction of iRFP713 transgenic reporter mice.

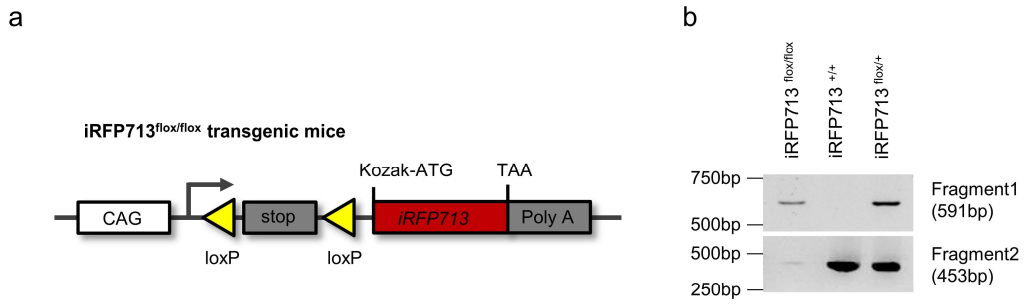

(**a**) Genome structure of the pCAG-loxP-stop-loxP-iRFP713 transgene in iRFP713$^{flox/flox}$ transgenic mice. The transgene consists of a CAG promoter, a loxP-flanked stop gene, followed by iRFP713. Cre-mediated recombination excises the floxed stop gene, resulting in the expression of iRFP713. (**b**) Genotyping PCR of iRFP713 transgenic mice, and independent triplicate experiments were repeated. Source data are provided as a Source Data file.

Supplementary Figure 5. The expression pattern of iRFP713 in different tissues of iRFP713 general expressing mice.

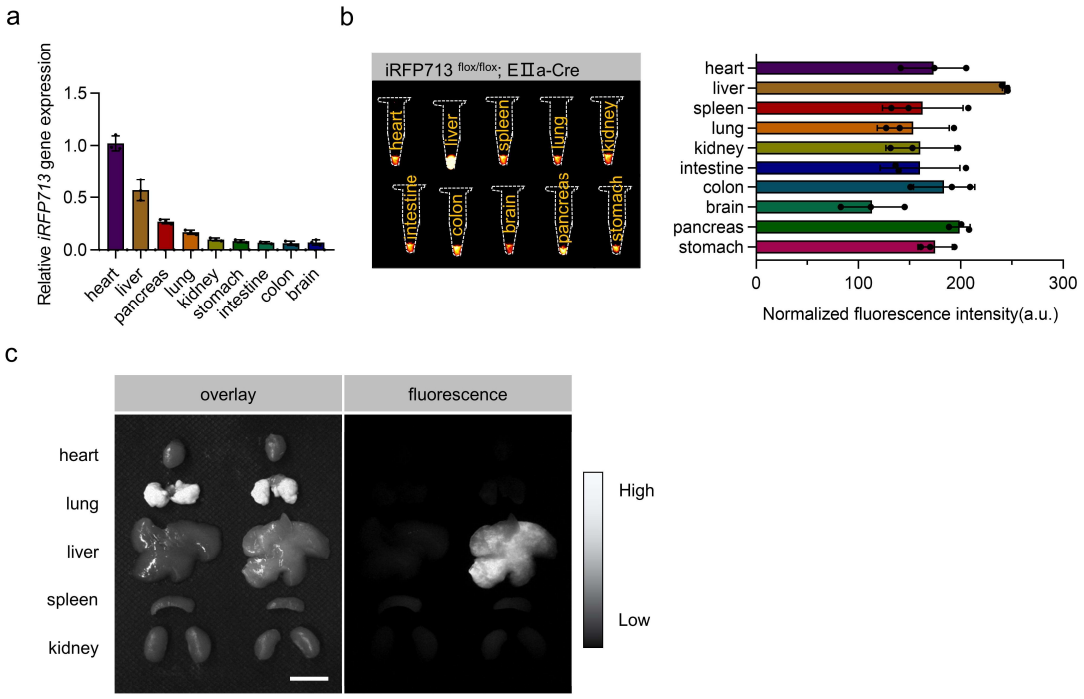

(**a**) *iRFP713* gene expression levels in different tissues of iRFP713$^{flox/flox}$; EIIa-Cre mice (n = 3 mice). (**b**) Representative NIR-II fluorescence images of different protein extracts from the various tissues of iRFP713$^{flox/flox}$; EIIa-Cre mice. Mean fluorescence intensities were normalized to per mg protein of each tissue and are shown on the right (n = 3 mice). (**c**) Representative overlay (NIR-II fluorescence + brightfield channel) and NIR-II fluorescence images of major organs isolated from littermate controls (left) and iRFP713$^{flox/flox}$; EIIa-Cre mice (right). All data presented as mean values ± SEM. Images were acquired using 690 nm excitation and 900 nm LP filters. Exposure times: 30 ms (**b**, **c**). Scale bar: 1 cm.

Supplementary Figure 6. Specific expression of iRFP713 in the liver of hepatocyte-specific iRFP713 expressing mice.

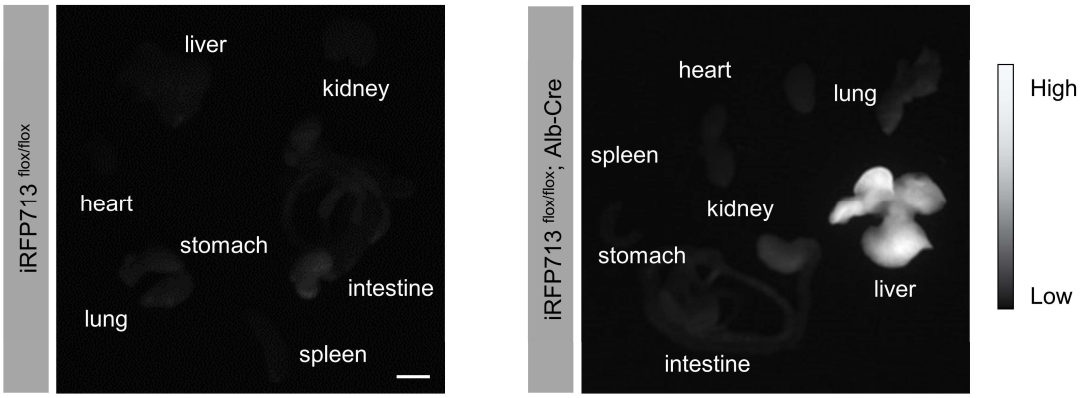

Representative NIR-II fluorescence images of major organs isolated from littermate controls (iRFP713$^{flox/flox}$) and hepatocyte-specific iRFP713 expressing mice (iRFP713$^{flox/flox}$; Alb-Cre). Isolated organs were imaged using 690 nm excitation and 900 nm LP filters. Exposure times: 15 ms. Scale bar: 1 cm.

Supplementary Figure 7. Liver morphology of the hepatocyte-specific iRFP713 expressing mice after partial hepatectomy (PHX).

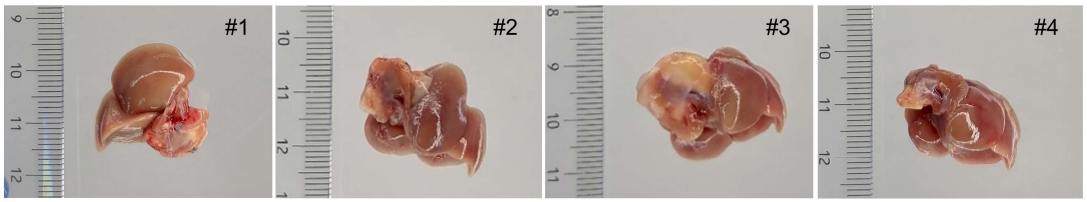

Liver resection model was established by removing the middle lobe and left lobe of iRFP713$^{flox/flox}$; Alb-Cre mice. Ten days after PHX, mice were sacrificed, livers were isolated, and gross liver morphology of each mouse was imaged. The numbers in the upper-right corner of each panel represents individual mice.

Supplementary Figure 8. Effect of iRFP713 expression on hepatocyte proliferation after PHX.

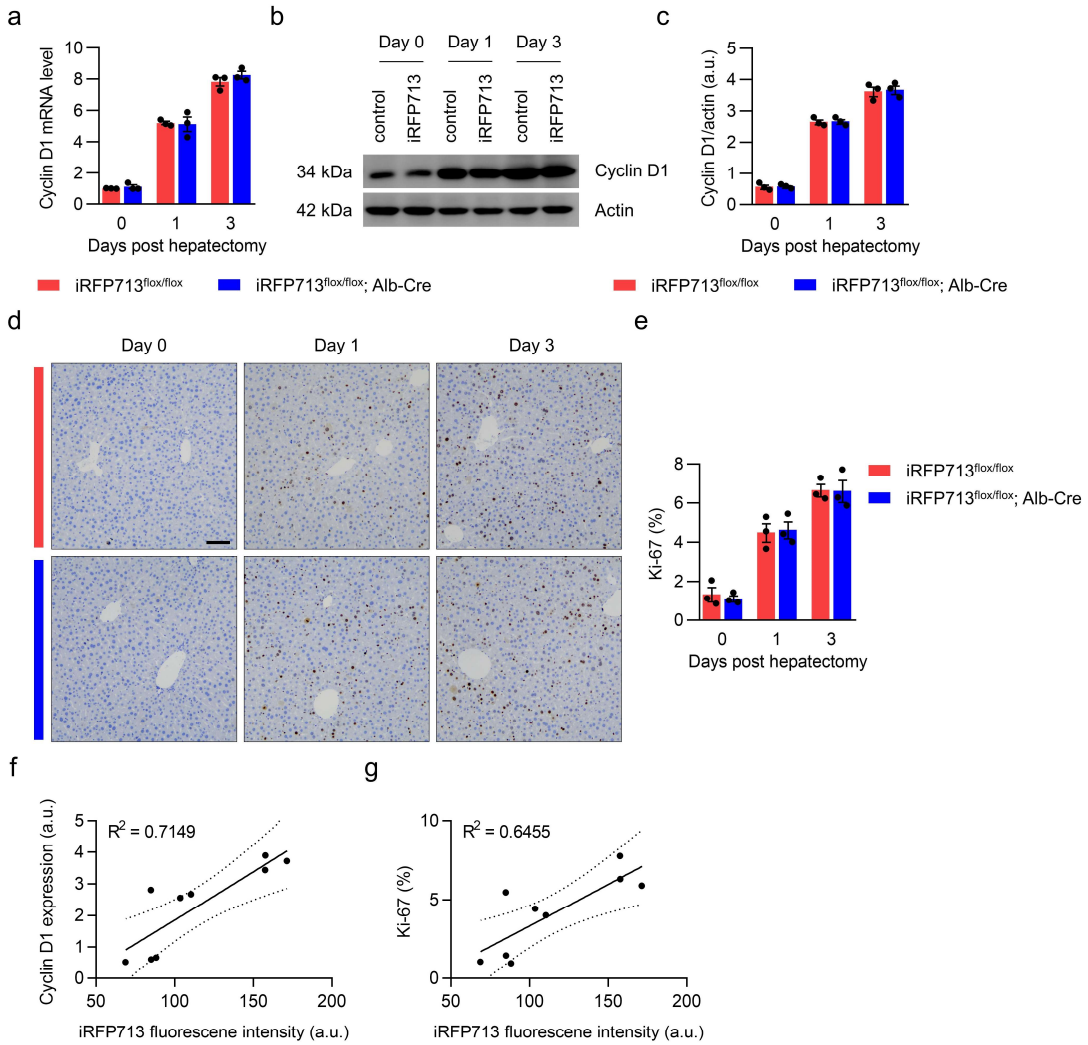

Liver was harvested from iRFP713$^{flox/flox}$ and iRFP713$^{flox/flox}$; Alb-Cre mice at day 0, day 1 and day 3 after PHX. (**a**) mRNA level (**b**) and protein level of cyclin D1, (**c**) intensities of cyclin D1 protein bands were quantified and normalized to actin (n = 3 mice). (**d**) Representative images and (**e**) quantification of IHC staining for Ki-67 (n = 3 mice). The correlations between iRFP713 fluorescence intensity and cyclin D1 protein expression (**f**), and Ki-67 staining (**g**), error bands display 95% confidence intervals. All data presented as mean values ± SEM. Scale bars: 20 μm (**d**). Source data are provided as a Source Data file.

Supplementary Figure 9. Hepatotoxicity and NIR-II fluorescence *in vivo* imaging of ICG.

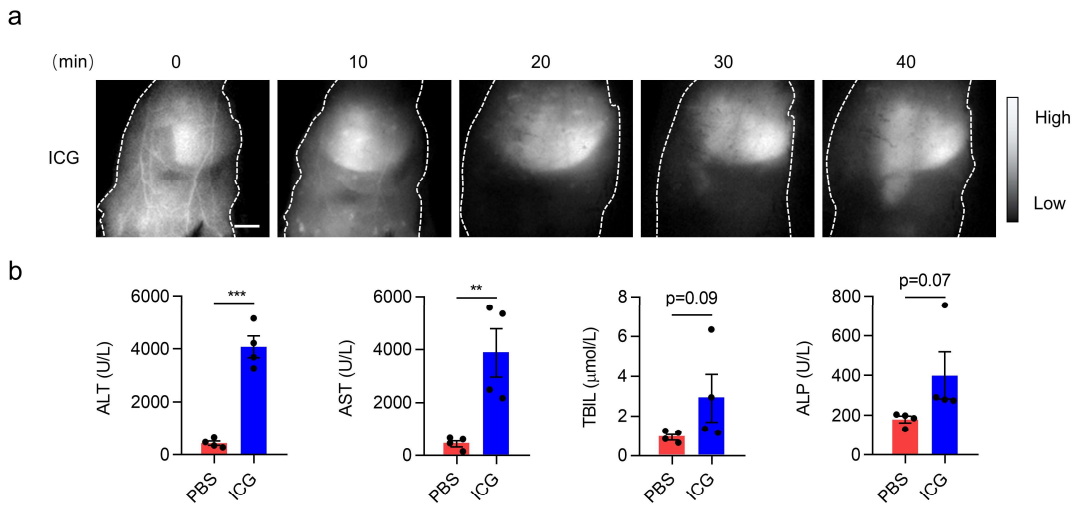

(**a**) Representative fluorescence images of C57BL/6 mice at different time points after intravenous injection of ICG (1 mg/mL). Images were recorded with 793 nm excitation and 900 nm LP collection. (**b**) Four main hepatic function indexes of ICG-treated mice. 6 to 8-week-old C57BL/6 mice underwent liver resection and were subsequently treated with ICG (1 mg/mL) or control PBS. After 24 hours, sera were collected from the mice for liver functional tests, including alanine transaminase (ALT, ***$p<0.001$), aspartate transaminase (AST, **$p<0.01$), total bilirubin (TBIL), and alkaline phosphatase (ALP). Data presented as mean ± SEM; n = 4 mice for each group. Statistical analysis were performed by unpaired two-tailed Student's t test. Exposure times: 15 ms. Scale bar: 5 mm.

Supplementary Figure 10. Comparation of liver proliferation and injury between iRFP713 and ICG.

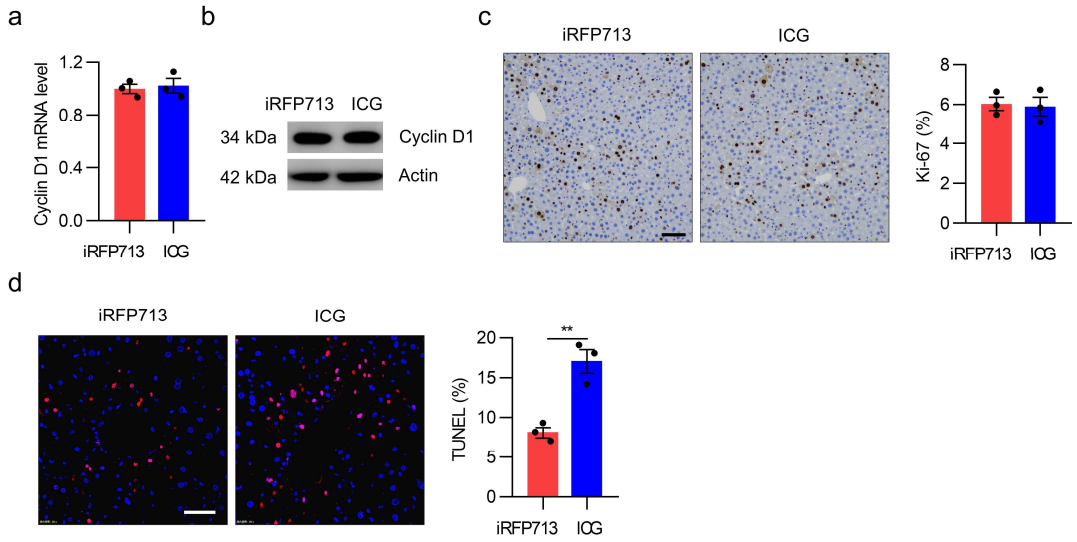

One day after PHX, iRFP713$^{flox/flox}$; Alb-Cre mice and ICG treated C57BL/6 mice were sacrificed, and liver tissues were isolated from the mice for proliferation and injury detection. (**a**) mRNA level and (**b**) protein level of cyclin D1. (**c**) Representative IHC images and quantification of Ki-67 staining on liver sections. (**d**) Representative merged fluorescence images (TUNEL, red and DAPI, blue) and quantification of TUNEL assay (**p<0.01). All data presented as mean ± SEM; n = 3 mice for each group. Statistical analysis were performed by unpaired two-tailed Student's t test. Scale bars: 10 μm (**c**) and 5 μm (**d**). Source data are provided as a Source Data file.

Supplementary Figure 11. Characterization of APAP toxicity model.

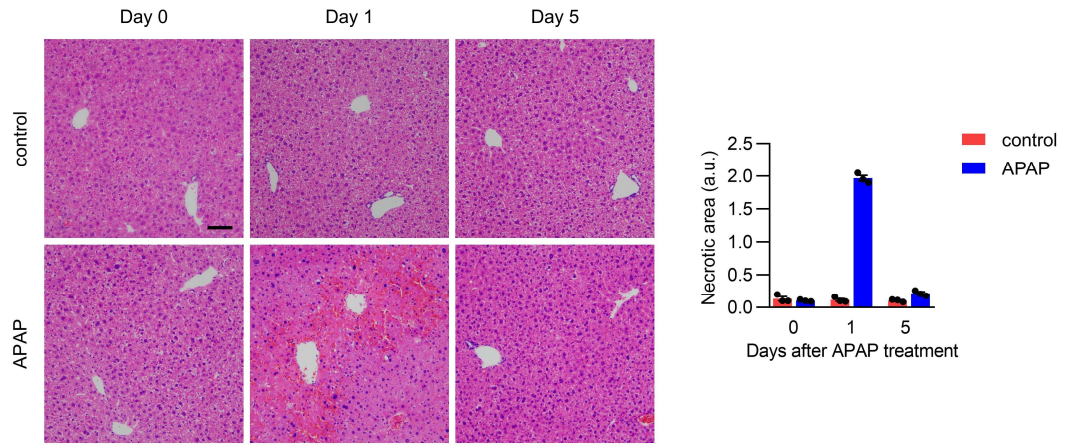

HE staining of liver isolated from iRFP713$^{flox/flox}$; Alb-Cre mice treated with or without APAP (250 mg/kg) at day 0, day 1 and day 5. Quantification of necrotic area was provided in the right. Data presented as mean ± SEM; n = 3 mice for each group. Scale bar: 20 μm.

Supplementary Figure 12. Liver injury and recovery of hepatocyte-specific iRFP713 expressing mice treated with APAP.

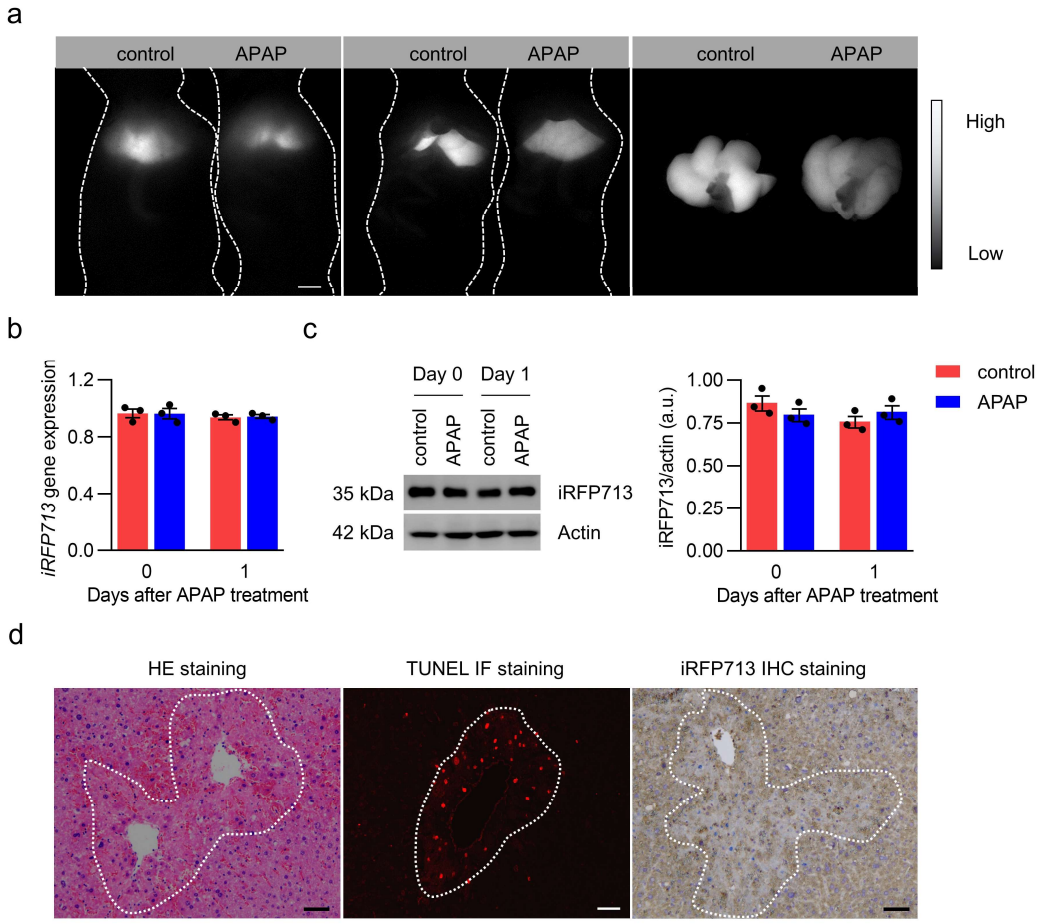

(**a**) Representative fluorescence images of iRFP713$^{flox/flox}$; Alb-Cre mice treated or not APAP. One day after APAP treatment, liver *in vivo* (**left**), liver with laparotomy (**middle**) and isolated liver (**right**) were imaged using 690 nm excitation and 900 nm LP filters. Exposure times: 10 ms (**a, left**), 50 ms (**a, middle**) and 20 ms (**a, right**). (**b**) iRFP713 gene expression level and (**c**) protein level in liver of iRFP713$^{flox/flox}$; Alb-Cre mice at day 0 and day 1 after treated or not APAP. Intensities of iRFP713 protein bands were quantified and normalized to actin (**c, right**). Data presented as mean ± SEM; n = 3 mice for each group. (**d**) Representative HE staining (**left**), TUNEL fluorescence staining (**middle**) and IHC staining of iRFP713 (**right**) in liver sections from iRFP713$^{flox/flox}$; Alb-Cre mice after 1 day of APAP treatment. These staining experiments were repeated independently three times with similar results. Scale bar: 5 mm (**a**), 20 μm (**d: left, right**), and 5 μm (**d: middle**). Source data are provided as a Source Data file.

Supplementary Figure 13. Characterization of multiple low-dose STZ induced diabetes.

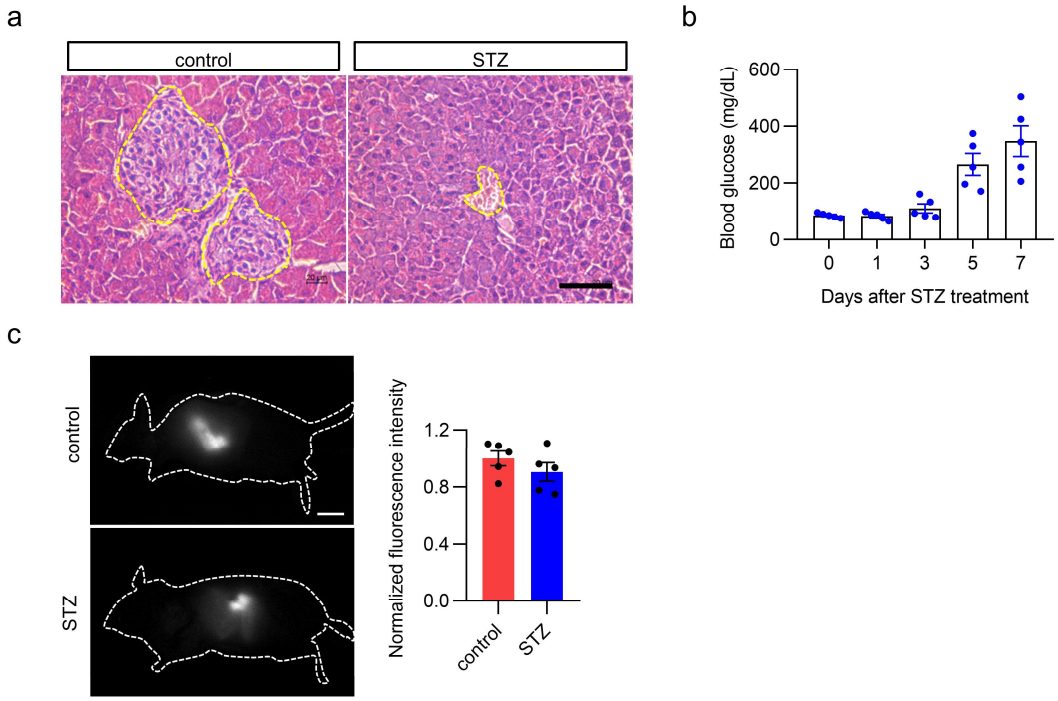

(**a**) Representative photographs of HE stained pancreas isolated from iRFP713$^{flox/flox}$; Pdx1-Cre mice treated with control saline (0.9% NaCl) or multiple low dose STZ (50 mg/kg/day, 5 days). (**b**) Blood glucose records of iRFP713$^{flox/flox}$; Pdx1-Cre mice at different times after STZ treatment. (**c**) Representative NIR-II fluorescence images of iRFP713$^{flox/flox}$; Pdx1-Cre mice treated with control saline or STZ. Mean fluorescence intensity was provided. All data presented as mean ± SEM; n = 5 mice for each group. Images were acquired with 690 nm excitation and 900 nm LP filters. Exposure times: 15 ms. Scale bars: 20 μm (**a**) and 5 mm (**c**).

Supplementary Figure 14. Long-term expression stability of iRFP713 transgenic mice.

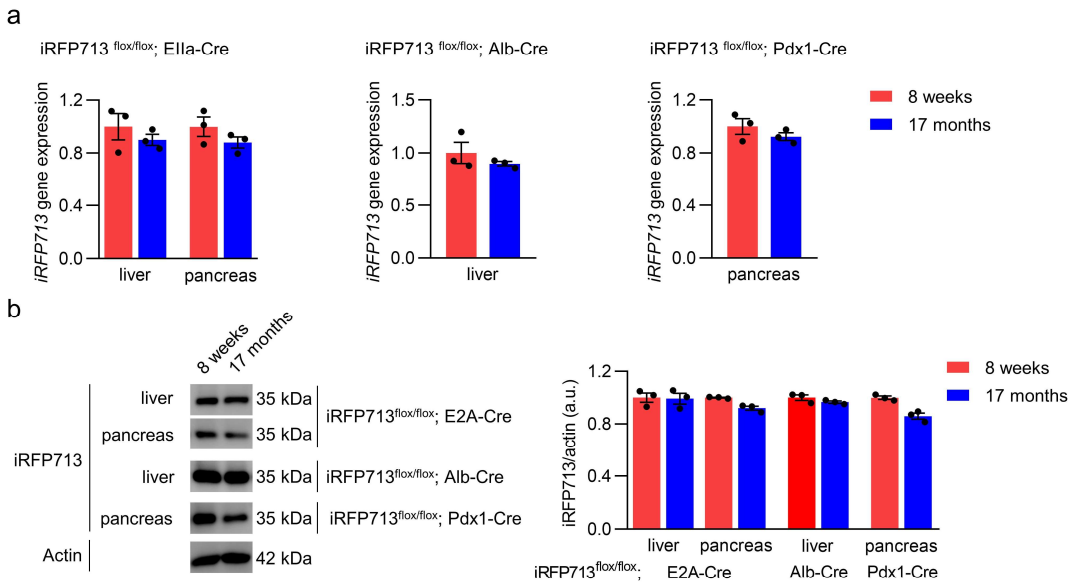

(**a**) Gene expression levels and (**b**) protein levels of iRFP713 in liver or pancreas of different iRFP713 transgenic mice (iRFP713$^{flox/flox}$; EIIa-Cre, iRFP713$^{flox/flox}$; Alb-Cre and iRFP713$^{flox/flox}$; Pdx1-Cre) at weeks 8 and months 17. iRFP713 protein bands intensities were quantified and normalized to actin (**b, right**). Data presented as mean ± SEM; n = 3 mice for each group. Source data are provided as a Source Data file.

Supplementary Figure 15. Comparison of iRFP713 imaging in NIR-I and NIR-II regions.

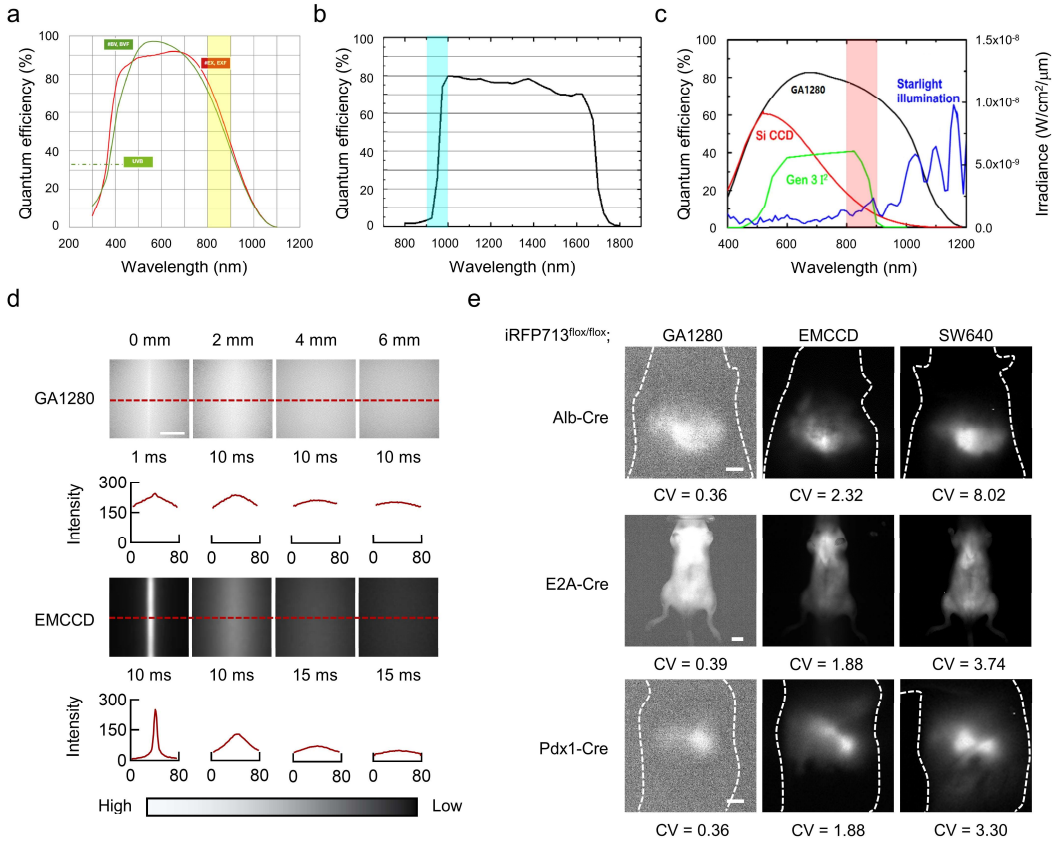

The quantum efficiency curve of (**a**) iXon Ultra 897 camera (EMCCD) and (**b**) SW640 camera (InGaAs FPA). The yellow area indicates the region of 800-900 nm and the blue area indicates the region of 900-1000 nm. (**c**) The quantum efficiency curve of GA1280 camera (vis-NIR 2D-detector, black line). The red area indicates the region of 800-900 nm. (**d**) NIR-I fluorescence (800-900 nm) images of a capillary tube containing iRFP713 immersed at various depths in 1% intralipid (1 mg mL^{-1}, 690 nm Ex). Exposure times: (GA1280) 0 mm: 1 ms; 2 mm, 4 mm and 6 mm: 10 ms. (EMCCD) 0 mm and 2 mm: 10 ms; 4 mm and 6 mm: 15 ms. (**e**) The NIR-I fluorescence (800-900 nm) images using the GA1280 camera (**left**) and iXon Ultra 897 camera (**middle**) and the NIR-II fluorescence (>900 nm) images using the SW640 camera (**right**). (690 nm Ex and 800-900 nm/>900 nm Em). Exposure times: (GA1280) Alb-Cre and Pdx1-Cre: 0.025 ms; E2A-Cre: 0.25 ms. (EMCCD) Alb-Cre, Pdx1-Cre and E2A-Cre: 1 ms. (SW640) Alb-Cre: 5 ms; E2A-Cre: 10 ms; Pdx1-Cre: 1 ms. Scale bars: 5 mm (**d, e**).

Supplementary Table 1. The calculated area SBR values.

Area SBR values	GA1280	iXon Ultra 897	SW640
iRFP713$^{flox/flox}$; Alb-Cre	3.07	21.62	213.99
iRFP713$^{flox/flox}$; E2A-Cre	2.33	13.32	72.31
iRFP713$^{flox/flox}$; Pdx1-Cre	2.95	17.83	47.07

Supplementary Table 2. Primers of iRFP713.

Genotyping primers	
Primers	**Sequence (5'-3')**
iRFP713-F	CACTTGCTCTCCCAAAGTCGCTC
iRFP713-R1	ATACTCCGAGGCGGATCACAA
iRFP713-R2	AGATGTACTGCCAAGTAGGAAAGTC
RT-qPCR primers	
Primers	**Sequence (5'-3')**
iRFP713-qPCR-F1	CACTCTTCCATCACGCCGAT
iRFP713-qPCR-R1	TGATCGTTTGCCATCACCGA

Supplementary Table 3. Antibodies used for experiments.

Antibody	Catalog Number	Company	Dilution
Cyclin D1	60186-1-Ig	Proteintech	1:1000
Ki-67	556003	BD Biosciences	1:500
Actin	4970	Cell signaling technology	1:5000
iRFP713	Not available	HuaAn Biotechnology	1:1000